Aging and reactivity assessment of nanoscale zerovalent iron in groundwater systems

Junmin Deng, Tao Chen, Yara Arbid, Mathieu Pasturel, Sungjun Bae, Khalil Hanna

Aging and reactivity assessment of nanoscale zerovalent iron in groundwater systems

Junmin Deng[a], Tao Chen[a], Yara Arbid[a], Mathieu Pasturel[a], Sungjun Bae[b], Khalil Hanna[a*]

[a] *Univ. Rennes, Ecole Nationale Supérieure de Chimie de Rennes, CNRS, ISCR-UMR 6226, F-35000 Rennes, France*

[b] *Department of Civil and Environmental Engineering, Konkuk University, 120 Neungdong-ro, Gwangjin-gu, Seoul 05029, Republic of Korea*

*Corresponding author: khalil.hanna@ensc-rennes.fr

Abstract

In this study, changes in the reactivity of nanoscale zerovalent iron (NZVI) in five different groundwater (GW) systems under anoxic and oxic conditions were examined over a wide range of aging time (0−60 d). *p*-nitrophenol (*p*-NP) was used as a redox-sensitive probe, whereas nalidixic acid (NA), a typical antibiotic found in the natural environment, was used as a sorbing compound. Investigation of the *p*-NP reduction in pure water systems showed that NZVI lost 41% and 98% of its reductive activity under anoxic and oxic conditions after 60 d, while enhancement of its reactivity was observed after short-term aging in GW (1−5 d), followed by a further decline. This behavior has been ascribed to the formation of secondary Fe(II)-bearing phases, including magnetite and green rust, resulting from NZVI aging in GW. Adsorption experiments revealed that GW-anoxic-aged NZVI samples exhibited a good affinity toward NA, and a greater NA adsorption (~27 μmol g^{-1}) than that of pristine NZVI (~2 μmol g^{-1}) at alkaline pH values. Surface complexation modeling showed that the enhanced adsorption of NA onto secondary minerals can be attributed to the Fe(II)-NA surface complexation. This considerable change in the reductive ability and the adsorption capacity of NZVI arising from groundwater corrosion calls for greater attention to be paid in assessment studies, where NZVI is injected for long-term remediation in groundwater.

Keywords: NZVI; aging effect; groundwater; reactivity; secondary minerals.

1. Introduction

Nanoscale zerovalent iron (NZVI) is one of the most extensively studied nanomaterials of environmental clean-up technologies (Li et al. 2017; Phenrat et al. 2016; Wei et al. 2010; Xia et al. 2017). Because NZVI is an environmentally safe material with high surface area and great reactivity, it has been widely applied in treatments of contaminants, including persistent organic compounds (Joo et al. 2004), toxic inorganic contaminants (Ryu et al. 2011), and even radioactive nuclides (Tsarev et al. 2017).

Despite NZVI having been frequently applied in *in-situ* groundwater remediation (Libralato et al. 2017; Mueller et al. 2012), the remedial performance of NZVI is sensitive to many geochemical factors in groundwater such as organic matter (Giasuddin et al. 2007; Zhou et al. 2022), cations (Chen et al. 2018), and anions (Su et al. 2012). For instance, inhibition of As(V) and As(III) removal by NZVI was reported in the presence of humic acid (Giasuddin et al. 2007), while the presence of Cl^-/SO_4^{2-}/Cu^{2+} enhanced the reduction of hexachlorobenzene (Su et al. 2012). Groundwater constituents may affect not only the NZVI reactivity but also its fate or mineralogical transformation over long-term aging in the natural environment. Indeed, NZVI can be completely or partially oxidized into various Fe(II)/Fe(III) (hydr)oxides depending on the groundwater conditions (Bae et al. 2018). In the presence of HCO_3^-, the formation of magnetite/carbonate green rust/iron carbonate hydroxide as aging products of NZVI

have been observed (Xie and Cwiertny 2012), whereas the presence of SO_4^{2-} enabled the formation of magnetite/schwertmannite (Reinsch et al. 2010). Further investigations of NZVI aging in synthetic groundwater revealed that magnetite was a major aging product with traces of goethite/amakinite under anoxic conditions (Schöftner et al. 2015), with lepidocrocite being the only iron phase found after 60 d aging under oxic conditions (Dong et al. 2012). However, a comprehensive understanding of short- and long-term aging effects on NZVI behavior in real groundwater is still limited. Despite very few investigations (Adeleye et al. 2013) on the long-term environmental fate of commercial NZVI in groundwater, little is known about the reactivity of the generated secondary iron phases which can further influence interactions with co-existing contaminants.

Herein, a comprehensive kinetic assessment of reductive and adsorptive capacities of NZVI and aged NZVI in various real groundwater was performed under oxic and anoxic conditions to determine the NZVI reactivity versus corrosion over a wide range of aging time (0−60 d). Specifically, the main aim was to assess the interaction mechanisms of "aged" NZVI particles with *p*-nitrophenol (*p*-NP), a redox-sensitive probe, and nalidixic acid (NA), a sorbing antibiotic contaminant in natural systems. Five different groundwater samples from different places in France were used in this study. The reduction of *p*-NP by fresh NZVI in pure water (PW) and the five groundwater samples was first evaluated, and the mineral transformation of NZVI particles after the reaction was analyzed by X-ray diffraction (XRD) and high-

resolution transmission electron microscopy (HR-TEM). Structural and compositional analyses were performed for aging products at the desired aging time under anoxic and oxic conditions, and additional reduction experiments were performed to investigate the changes in the reductive activity of NZVI aging products. NA adsorption on the NZVI aging products was also evaluated as a function of pH, and a surface complexation model was developed to describe the impact of surface-bound Fe(II) of aged NZVI samples on NA adsorption.

2. Materials and methods

2.1. Chemicals and materials

Complete information on chemicals used in this study is presented in the Supporting Information (SI). NZVI (50−100 nm) was synthesized by following our previous method (Deng et al. 2020). It exhibited a typical chain-like core-shell structure as per high-resolution transmission electron microscopy (HR-TEM) analysis (Fig. S1). Maghemite (γ-Fe_2O_3, >99.0%) was purchased from Alfa Aesar (Ward Hill, MA, USA). Magnetite (Fe_3O_4) (Cheng et al. 2018), lepidocrocites (γ-FeOOH) (Paterson 2000), carbonate green rust ($[Fe^{2+}_4Fe^{3+}_2(HO)_{12}]^{2+}\cdot[CO_3^{2-}\cdot mH_2O]^{2-}$) (Williams and Scherer 2001) and goethite (α-FeOOH) (Xu et al. 2017a), were synthesized following the published methods. Five groundwater samples were collected in France at sites with

the following GPS locations: GW1 (48.02881, -1.47230), GW2 (48.02944, -1.47215), GW3 (45.71039, -0.00009), GW4 (45.70212, -0.00808), and GW5 (45.70209, -0.00895). Raw groundwater samples were filtered using 0.2 µm membranes (Whatman; Maidstone, Kent, UK) to remove solids and microbes.

The glasswares used for the reaction were soaked in 5% (v/v) HCl for at least 48 h and rinsed before use. Unless specifically stated, all solutions were prepared with deoxygenated deionized water (DDIW, 18.2 MΩ·cm) prepared by purging with nitrogen (N_2, 99.99%) for 4 h and stored in an anaerobic chamber (Jacomex, Dagneux, France).

2.2. Groundwater characterization

Physicochemical characteristics including pH, electrical conductivity (EC), total dissolved solids (TDS), total organic carbon (TOC), total hardness (TH), total phosphate (TP), common anions, and cations (Table S1) of the groundwater samples were measured following the guidelines of "Standard Methods For The Examination of Water and Wastewater American Public Health Association" (Eaton et al. 1966). Particularly, anions in groundwater were determined using ion chromatography (IC; Dionex Corp., Sunnyvale, CA, USA), while cations were measured by inductively coupled plasma mass spectrometry (ICP-MS, Agilent 7700x; Agilent Technologies, Santa Clara, CA, USA). The pH and EC were determined using a pH meter (HANNA,

127 HI991003; Hanna Instruments, Smithfield, RI, USA) and a conductivity meter LF 340
128 (WTW, Weilheim, Germany), respectively. Total hardness was determined by the
129 EDTA titration method, and TDS was measured gravimetrically (Patnaik 2017). Silicate
130 and phosphate analyses were performed according to the molybdenum blue method
131 (Grasshoff et al. 2009), and the ammonium molybdate spectrometric methods (Standard
132 and ISO 2004), respectively. The concentration of carbonate species was measured by
133 the acid titration method (Eaton et al. 1966).
134

135 *2.3. Characterizations of NZVI and aged NZVI particles*

136 The aged NZVI was prepared by using NZVI (10 g L^{-1}) suspensions in 15-mL vials
137 containing DDIW or deoxygenated GW1. Subsequently, the NZVI suspension was
138 placed under ambient air condition (oxic aging) or in an anaerobic chamber (anoxic
139 aging) and allowed to age for 1, 5, 15, 30, and 60 d. Given that the particles settle in the
140 vial with increasing aging time, thus potentially reducing the contact time with water,
141 the suspensions were vigorously mixed by hand shaking once a day (Dong et al. 2018).
142 The pH variation during aging was monitored using a portable pH meter. Aged NZVI
143 particles were separated by centrifugation at the desired aging time and dried in a
144 vacuum freeze drier (-52 °C, 24 h) for further characterization and experiments.
145 XRD (Bruker D8 Advance, Cu Kα1 radiation, λ = 1.5406 Å) was used to identify
146 the aging products of NZVI. The samples were transferred to sample holders and treated

147 with 1: 1 (v/ v) glycerol solution to avoid surface oxidation during the XRD analysis
148 (Bae and Lee 2014). The morphological information of aged NZVI particles was
149 obtained by HR-TEM (JEM-2100; JEOL, Tokyo, Japan) with selected area electron
150 diffraction (SAED). The dried NZVI aging products were transferred to ethanol
151 solution and sonicated for 30 min. Finally, a drop of the diluted suspension was placed
152 on the copper TEM grid and analyzed at an acceleration voltage of 200 kV.
153

154 *2.4. Reduction and adsorption experiments*

155 Experiments to measure the reactivity of fresh NZVI in different waters were
156 carried out in 200-mL flasks in an anaerobic chamber to avoid the effect of dissolved
157 oxygen during the reaction. An exact amount (1 mL) of 20 mM *p*-NP stock solution
158 was transferred to the flask containing 200 mL of filtered groundwater or DDIW,
159 followed by stirring at 500 rpm to prepare an initial *p*-NP concentration of 0.1 mM.
160 Then, 10 mg of NZVI was introduced into the solution to initiate the reduction of *p*-NP
161 by NZVI. At each sampling time, 1 mL of the sample was taken from the suspension
162 and filtered through a 0.2-μm filter (Whatman) for high-performance liquid
163 chromatography (HPLC) analysis.
164 Similar procedures were conducted to investigate the reductive activity of aged
165 NZVI particles. Briefly, aged NZVI suspension (10 g L^{-1}) was firstly bath-sonicated for
166 1 h. The aged NZVI suspension (1 mL) was added to 200 mL of *p*-NP solution (0.1

167 mM). Then, samples were taken at the desired time intervals and analyzed by HPLC.
168 In contrast to the reduction experiments, adsorption batch experiments of NZVI aging
169 products were initiated by transferring 10 mg of aged NZVI particles into 200 mL of
170 NaCl solution (10 mM). The pH was then adjusted to the required value using 0.1 M
171 and/or 1 M NaOH/HCl solutions. After 2 h of adsorption, an aliquot was taken and
172 filtered (0.2-μm, Whatman) to measure NA and dissolved Fe(II). To investigate the role
173 of each mineral phase on the reactivity of aged NZVI, additional reduction and
174 adsorption assessments of iron-containing minerals (*i.e.*, magnetite, maghemite,
175 carbonate green rust, lepidocrocite, and goethite, 50 mg L^{-1}) were carried out following
176 the same procedures described above. All experiments in this study were performed in
177 triplicate, and the data reported here were the average of the three replicated
178 experiments, and error bars represent the relative standard deviation.
179

180 *2.5. Analytical Methods*

181 The aqueous concentration of *p*-NP, *p*-AP, and NA were determined using an HPLC
182 (Waters 600 controller; Waters Corporation, Milford, MA, USA) equipped with a
183 photodiode array detector (Waters 996; Waters Corporation) and a reversed-phase C18
184 column (250 mm × 4.6 mm; *i.d.*, 5 μm). The UV detector was set to 273, 317, and
185 258 nm for *p*-NP, *p*-AP, and NA analyses, respectively (Bae et al. 2016, Xu et al. 2017c).
186 The mobile phase (mixture of acetonitrile/water (50/50, v/v) containing 0.1% formic

187 acid) was prepared and used at the flow rate of 1 mL min^{-1} in the isocratic mode for the
188 measurement of *p*-NP, *p*-AP, or NA. The dissolved Fe(II) concentration was measured
189 using the 1,10-phenanthroline method at a wavelength of 510 nm with a UV-vis
190 spectrophotometer (U-3310, Hitachi; Hitachi Ltd., Tokyo, Japan) (Fadrus and Malý
191 1975).
192

193 *2.6. Surface complexation modeling*

194 The NA adsorption by NZVI aging products at different pH values was described
195 using surface complexation modeling. The geochemical speciation code PHREEQC
196 and the "Minteq" database were used (D. L. Parkhurst and C. A. J. Appelo 1999). The
197 pK_a of NA is 6.19, and the logarithm of the formation constant of NA−Fe^+ (aq) is 3.99
198 (Vincent et al. 1981). The surface complexation model for iron oxides was used, as
199 previously reported, and the protonation of Fe surface sites was formulated following a
200 2-pK_a approach (Eq. 1 and 2) (Cheng et al. 2018, Hanna, 2007).

201 $$\equiv FeOH_2^+ \leftrightharpoons \equiv FeOH + H^+; pKa_1 \quad (1)$$

202 $$\equiv FeOH \leftrightharpoons \equiv FeO^- + H^+; pKa_2 \quad (2)$$

203 The charge-potential relationship was described according to the constant
204 capacitance model (CCM), and the modeling parameters are presented in Table S2. We
205 adapted the parameters of the three plane model (TPM) to use the CCM in PHREEQC
206 (version 2) (Cheng et al. 2018).

3. Results and discussion

3.1. *Reduction of p-NP by NZVI suspensions in various groundwater systems*

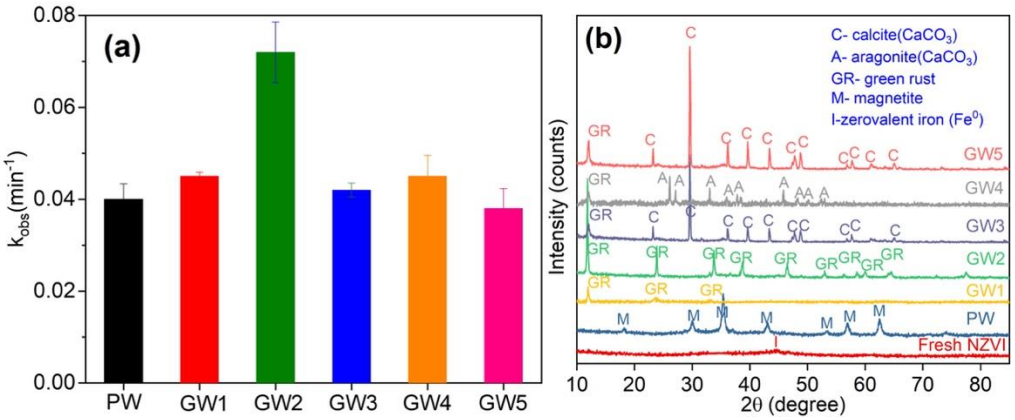

Figure 1. (a) Pseudo-first-order kinetic rate constants (k_{obs}, min^{-1}) of *p*-NP reduction by fresh NZVI in various water matrices, and (b) XRD data of corresponding solids. Experimental conditions: $[p\text{-NP}]_{initial}$ = 0.1 mM, [NZVI]= 50 mg L^{-1}, pH=9.0±0.2. Correlation coefficient (r^2) ranges from 0.95 to 0.99.

The removal kinetics of *p*-NP in various water matrices showed that *p*-NP was completely removed by NZVI within a 2 h-reaction in all experiments under anoxic conditions (Fig. S2). The aqueous concentrations of *p*-AP after the reaction revealed a complete mass balance of the conversion reaction of *p*-NP into *p*-AP (Table S3), indicating the negligible adsorption of *p*-NP or *p*-AP on NZVI surfaces in this study. The pseudo-first-order kinetic rate constants (k_{obs}, min^{-1}) were determined by considering the early stage of kinetics data over 30 min of reaction time (Fig. 1a). The

222 highest rate constant was observed in GW2 (0.07 min^{-1}), compared to PW and other
223 groundwater systems.

224 In contrast to the black color of NZVI in the PW system, a change of suspension
225 color to bluish-green was observed in the groundwater samples. The XRD analysis
226 revealed various corrosion products of NZVI depending on the water matrix (Fig. 1b).
227 In PW, diffraction peaks were observed at 18.4°, 30.2°, 35.5°, 43.2°, 53.6°, 57.2°, and
228 62.8°; these peaks can be assigned to maghemite (γ-Fe_2O_3)/magnetite (Fe_3O_4).
229 Carbonate green rust was detected in all groundwater systems, together with calcite in
230 GW3 and GW5 and aragonite in GW4 (Fig. 1b) (Dong et al. 2020, Kontoyannis and
231 Vagenas 2000).

232 The pH and concentration of the main dissolved species including anions and TOC
233 in the five groundwater matrices were determined after the reaction (Table S4). The
234 suspension pH in groundwater systems increased to approximately 9, owing to the
235 anaerobic corrosion of NZVI ($Fe(0) + 2H_2O \rightarrow Fe^{2+} + 2OH^- + H_2$) (Deng et al. 2020).
236 As the distribution of carbonate species is strongly dependent on the pH value (Fig. S3),
237 an increase in CO_3^{2-} species is expected, which can result in the formation of carbonate-
238 bearing minerals (e.g., $CaCO_3$ and carbonate green rust). The precipitation of $CaCO_3$
239 occurred mainly in GW3, GW4, and GW5 systems because of the relatively higher
240 initial concentration of calcium (2.44–2.61 mM) and bicarbonate (4.2–4.3 mM) (Table
241 S1). Indeed, a drop in the aqueous concentration of dissolved carbonates was observed,
242 especially in GW3, GW4, and GW5, which was comparable to the Cl^- and SO_4^{2-}

concentrations after the reaction (Table S4). Up to 88% of the initial NO_3^- concentration was eliminated in groundwater samples after the reaction, likely because of the reductive removal of NO_3^- by NZVI (Hwang et al. 2011; Su et al. 2014). For silicate concentration, up to 90% loss was detected after the reaction, probably due to its strong binding affinity toward iron minerals (Kanematsu et al. 2018). However, no significant change in Total Organic Carbon (TOC) was observed before and after reaction with NZVI (Table S4).

In contrast, the NZVI corrosion products, particularly Fe(II)-containing minerals, could further contribute to the reduction of *p*-NP. Indeed, previous studies have reported the greater reductive ability of green rust than that of magnetite (Digiacomo et al. 2020, Usman et al. 2018). An independent set of experiments using synthetic Fe-minerals confirmed that carbonate green rust led to 43% of *p*-NP removal in 5 h, whereas only 8% of *p*-NP was removed by magnetite, and almost no removal of *p*-NP by Fe(III)-oxyhydroxides was observed (Fig. S4). Therefore, the carbonate green rust generated in NZVI-groundwater suspensions could additionally reduce *p*-NP. Other groundwater constituents, such as nitrate and silicate, may decrease the *p*-NP reduction efficiency owing to the inhibitory effects caused by the competitive reduction reaction of nitrate with *p*-NP (Alowitz and Scherer 2002, Westerhoff and James 2003), and the blocking of the reactive sites by silicate (Meng et al. 2002). This may explain why the highest rate constant for *p*-NP reduction was observed for GW2, which contained a lower nitrate concentration. Nevertheless, to avoid the formation of $CaCO_3$ phases, which

could potentially interfere with the NZVI aging process, GW1 was selected and used for the kinetic assessment (reduction and adsorption) of aged samples.

3.2. *Effects of NZVI aging products on the reduction of p-NP*

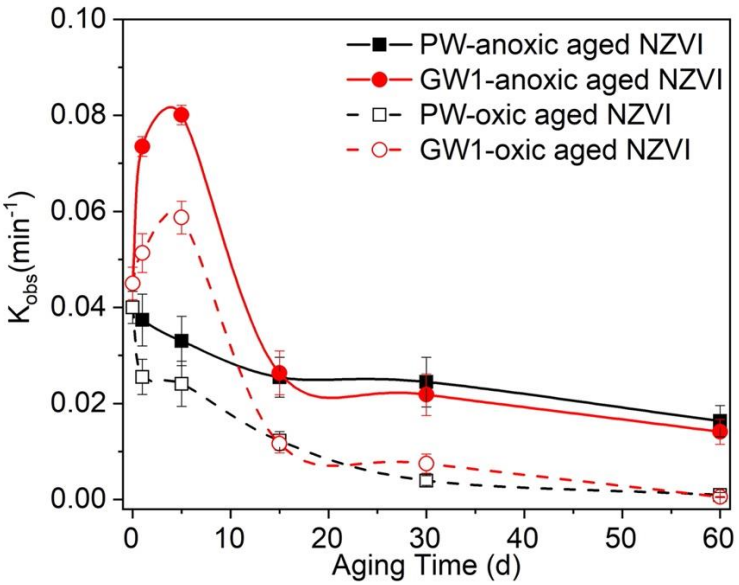

Figure 2. Variation of pseudo-first-order kinetic rate constants (k_{obs}, min^{-1}) of *p*-NP reduction with the aging time of differently aged NZVIs. Experimental conditions: [*p*-NP]$_{initial}$ = 0.1 mM, [NZVI]= 50 mg L^{-1}, reaction pH=9.0±0.2. GW: groundwater; PW: pure water. Correlation coefficient (r^2) ranges from 0.95 to 0.99.

Kinetics of removal of *p*-NP by different aged NZVI particles were monitored to check the impact of aging time on the overall reduction ability of NZVI suspension (Fig. S5). For PW systems, k_{obs} values continuously decreased as the aging time increased

under both anoxic and oxic conditions (Fig. 2). Almost 50% of *p*-NP was reduced into *p*-AP in the 60 d-aging sample under anoxic conditions, while no reduction was observed for the 60 d-aged samples under oxic conditions (Fig. S5). A bell-shaped curve was observed for k_{obs} variation with aging time for GW1-aged NZVI; *i.e.,* k_{obs} values increased over the early stage of aging (0–5 d) and then decreased with further aging. In particular, the reductive ability of NZVI in groundwater reached a maximum after 5 d aging, which was much higher (~1.8 times) than that of the fresh materials. In general, the samples of anoxic-aged NZVI showed better *p*-NP reduction than that of the oxic-aged NZVI. Similar trend of NZVI reactivity against aging time in simulated groundwater under anoxic conditions has been previously reported (Xiao et al. 2022). This behavior could be explained by the preservation of fresh NZVI and/or the occurrence of more reactive Fe phases under anoxic conditions.

In order to assess the phase transformation of NZVI in PW and GW1 systems, XRD analyses of secondary iron minerals were conducted under oxic and anoxic conditions (Fig. 3). The abundance of the α-Fe phase decreased gradually for all the samples. For PW-anoxic-aged NZVI, the XRD peaks of Fe(0) remained until 5 d, and magnetite/maghemite was detected as the main aging product (Fig. 3a), while the disappearance of the Fe(0) peak coupled with the appearance of carbonate green rust and magnetite/maghemite was observed in the 5 d-aged sample of PW-oxic-aged NZVI (Fig. 3c). In contrast, peaks of carbonate green rust and magnetite/maghemite were detected in GW1-anoxic-aged NZVI, with the disappearance of Fe(0) observed at

longer aging times (Fig. 3b). In GW1-oxic-aged NZVI, an increase in peaks of carbonate green rust and magnetite/maghemite was observed at only 1 d of aging (Fig. 3d). Then, a significant increase in Fe(III)-oxyhydroxides (lepidocrocite and/or goethite) with a decrease in peaks of carbonate green rust at 60 d was observed, suggesting the conversion of carbonate green rust into lepidocrocite and/or goethite under oxic conditions (Legrand et al. 2004, Schwertmann and Fechter 1994). More details about the changes in solution chemistry and pH values of NZVI suspensions along the aging process are given in the SI (Fig. S6).

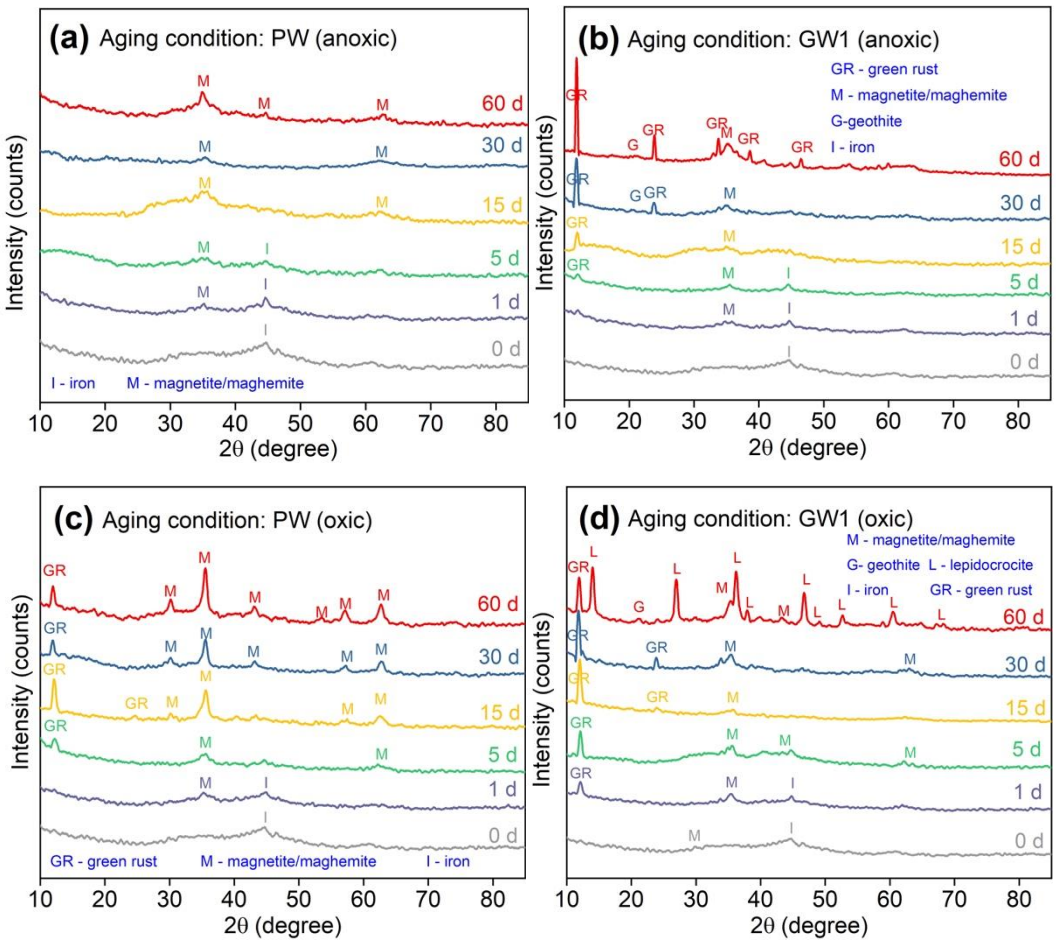

Figure 3. XRD pattern of fresh and NZVI aging products: (a) PW-anoxic-aged NZVI, (b) GW1-anoxic-aged NZVI, (c) PW-oxic-aged NZVI, and (d) GW1-oxic-aged NZVI.

311 Experimental conditions: $[p\text{-NP}]_{initial}$ = 0.1 mM, [NZVI]= 50 mg L^{-1}, reaction
312 pH=9.0±0.2. GW: groundwater; PW: pure water.
313
314 Collectively, these results showed that NZVI gradually lost its reactivity under both
315 anoxic and oxic conditions in the PW system, probably due to the consumption of Fe(0)
316 and accumulation of an oxyhydroxide layer coating the NZVI surface. In groundwater
317 systems, though an initial enhancement of *p*-NP removal was observed over a short
318 aging time (1−5 d), a decline was observed at later aging times. The greater reduction
319 ability of carbonate green rust compared to that of magnetite, maghemite, lepidocrocite,
320 or goethite (see Fig. S4) may explain the higher k_{obs} values observed in groundwater
321 systems over the initial aging period. Previous work has also shown that the breakdown
322 of the iron oxide shell coating of the ZVI may occur during the early stage of aging,
323 thereby allowing better access to the core Fe(0) (Xie and Cwiertny 2012). Furthermore,
324 as previously reported, the divalent cationic metal contained in groundwater may bind
325 to surface coatings and induce surface oxide layer dissolution or NZVI depassivation
326 (Liu et al. 2014).
327

3.3. *Effects of NZVI aging products on the adsorption of nalidixic acid*

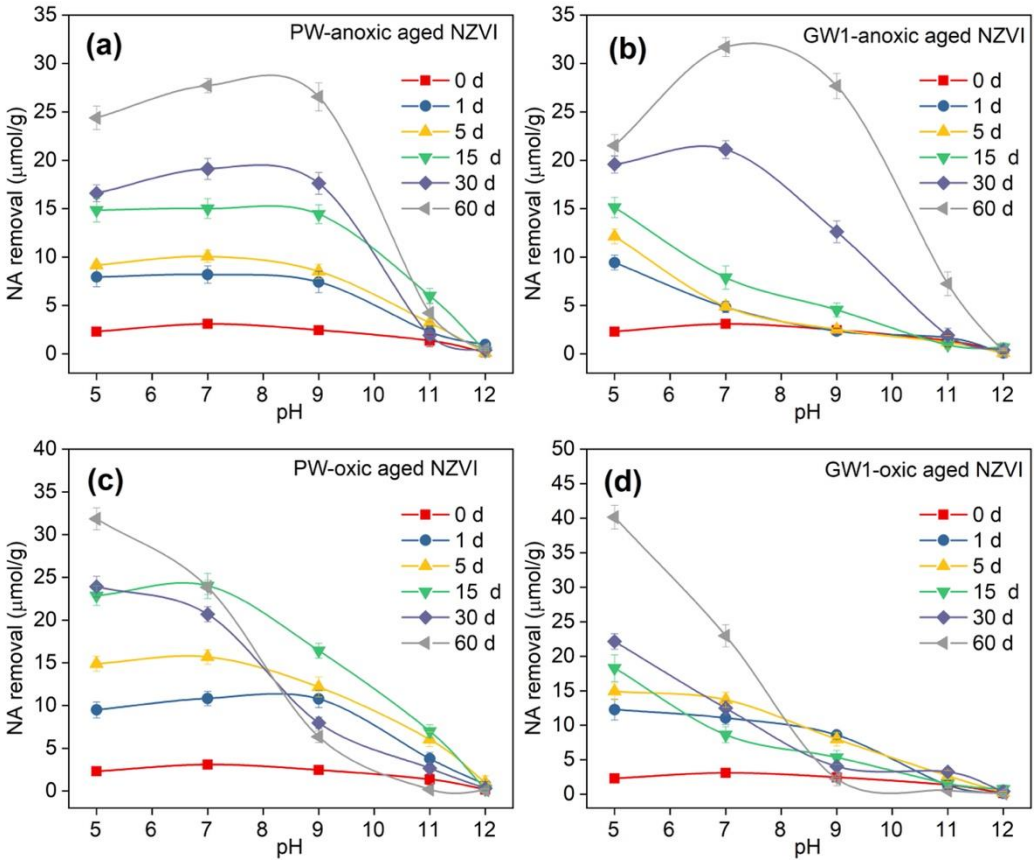

Figure 4. Nalidixic acid adsorption versus pH by fresh and different aged NZVI samples: (a) PW-anoxic-aged NZVI, (b) GW1-anoxic-aged NZVI, (c) PW-oxic, and (d) GW1-oxic. Experimental conditions: $[NA]_{initial}$ = 10 μM, [NZVI]= 50 mg L^{-1}, adsorption duration = 2 h. GW: groundwater; PW: pure water.

NA adsorption to differently aged NZVI particles was investigated over a wide pH range (5−12) (Fig. 4). The NA adsorption of NZVI aging products generally increased with increasing aging time, especially under acidic/neutral conditions. However, a different scenario of NA adsorption was observed for groundwater-aged NZVI samples.

NA adsorption by GW1-anoxic-aged NZVI decreased sharply as the pH increased, but the adsorption envelope exhibited a bell-shaped curve with increasing aging time. In contrast, GW1-oxic-aged NZVI exhibited an inversed S-shaped adsorption curve.

Considering the different binding affinity of NA to different iron minerals (Cheng et al. 2018, Xu et al. 2017b), this adsorption behavior by aged NZVI could be attributed to the change in mineral composition of NZVI aging products. The adsorption capacity of individual Fe oxyhydroxides, including magnetite, maghemite, carbonate green rust, lepidocrocite, and goethite, were evaluated over the same pH range (5−12) (Fig. S7). A negligible amount of NA was adsorbed by fresh NZVI, whereas Fe-(hydro)oxides exhibited significant NA adsorption capacity, especially in acidic to neutral pH. Under alkaline conditions, green rust exhibited better NA adsorption performance (when the adsorbed amount was normalized to mass and not surface area) than magnetite. However, a quantitative comparison of adsorption capacities must be made with caution since these synthetic minerals have different properties, including crystallinity, specific surface area, and surface charge.

According to the shape of the NA adsorption envelope (Fig. S7), more adsorption at circumneutral pH was observed with Fe(II)-Fe(III) mixed valent minerals (*e.g.*, magnetite and carbonate green rust), while Fe(III) bearing minerals (*e.g.*, lepidocrocite, goethite, and maghemite) exhibited an S-shaped curve or downward trend. Generally, organic ligands binding to metal-oxides show maximum adsorption at a pH near the pKa value (6.19 for NA). Indeed, previous reports showed typical NA adsorption by

Fe-oxides with maximum NA adsorption at pH around 6 (Robberson et al. 2006, Xu et al. 2017b). However, the pH-adsorption curve of NA shifted to larger pH values in the case of magnetite and green rust, probably because of the presence of released Fe(II) in solution. As previously observed for magnetite, the addition of dissolved Fe(II) in suspension increased the NA adsorption at neutral to alkaline pH values (Cheng et al. 2018). Here, Fe(II) release during NA adsorption was monitored for the 60 d-aged sample and presented in Fig. S8. Ferrous ion release was detected in all cases at pH 5 and 7 and became negligible at pH above 9. Interestingly, the pH dependence of NA adsorption is fully consistent with that of dissolved Fe(II) concentration. For instance, a high dissolved Fe(II) amount was observed for anoxic-aged NZVI samples, which exhibited greater adsorption performance even at high pH values. PW-oxic-aged NZVI samples showed more NA adsorption than GW-oxic-aged NZVI under alkaline conditions. This correlation suggests that the amount of dissolved Fe(II) or the mineral bound-Fe(II) plays a key role in NA adsorption behavior onto NZVI secondary phases.

3.4. Surface complexation modeling for nalidixic acid binding onto the 60 d-aged sample

First, determining the mineral composition of the aged samples is a prerequisite to describing the NA binding to secondary iron phases. In this study, the most aged sample (60 d) was selected to determine the proportion of identified secondary minerals (see

381 Table S5). Almost 100% of the magnetite/maghemite phase was present in PW-anoxic-
382 aged NZVI, while GW1-anoxic-aged NZVI contained approximately 55% of
383 magnetite/maghemite, 10% of goethite, and 35% of carbonate green rust. For PW-oxic-
384 aged NZVI, magnetite/maghemite was the main aging product (~86%) with 14% of
385 carbonate green rust, while GW1-oxic-aged NZVI contained various Fe mineral phases
386 (magnetite/maghemite, ~55%; goethite, ~8%; carbonate green rust, ~7%; and
387 lepidocrocite, ~30%).
388

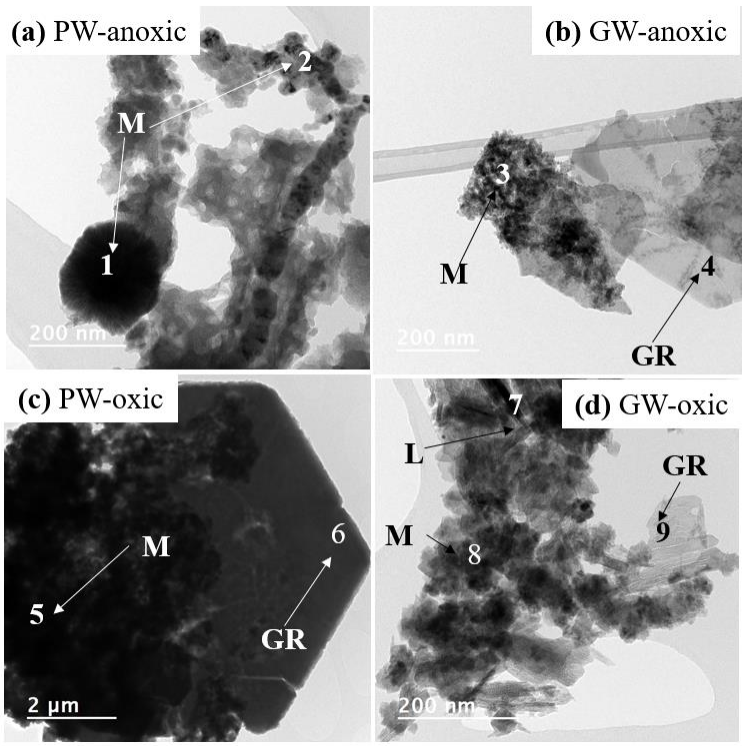

389
390 Figure 5. Transmission electron microscopy images of NZVI aging products at 60 days
391 under different conditions: (a) PW- anoxic system, (b) GW-anoxic system, (c) PW-oxic
392 system, and (d) GW-oxic system. Note: M: magnetite/maghemite; GR: green rust; L:
393 lepidocrocite; GW: groundwater; PW: pure water. (Electron diffraction patterns of the

394 numbered areas are presented in Fig. 6).

395

396 HR-TEM images confirmed that the initial chain-like aggregated structures and
397 large-sized spherical aggregates (approximately 200 nm) of NZVI (Fig. S1) were
398 transformed into magnetite/maghemite after 60 d of aging in a PW-anoxic system (Fig.
399 5a). In GW1-anoxic-aged NZVI samples, the particle size of magnetite/maghemite
400 decreased significantly (approximately 5 nm), and magnetite/maghemite seemed to be
401 attached to the surface of the hexagonal shape of carbonate green rust (Fig. 5b). Under
402 oxic conditions, carbonate green rust was observed in both PW- and GW1-aged
403 products (Figs. 5c, d). Particularly, the co-existence of magnetite with carbonate green
404 rust was detected in PW-oxic-aged NZVI samples, while needle-shaped particles of
405 lepidocrocite were observed in GW1-oxic-aged NZVI. All the SAED patterns of
406 specific Fe mineral phases in Figure 5 are also provided in Figure 6, which shows the
407 typical patterns of each mineral (Araújo-Neto et al. 2014, Génin et al. 2005, Krystofiak
408 et al. 2013, Liao et al. 2020).

409

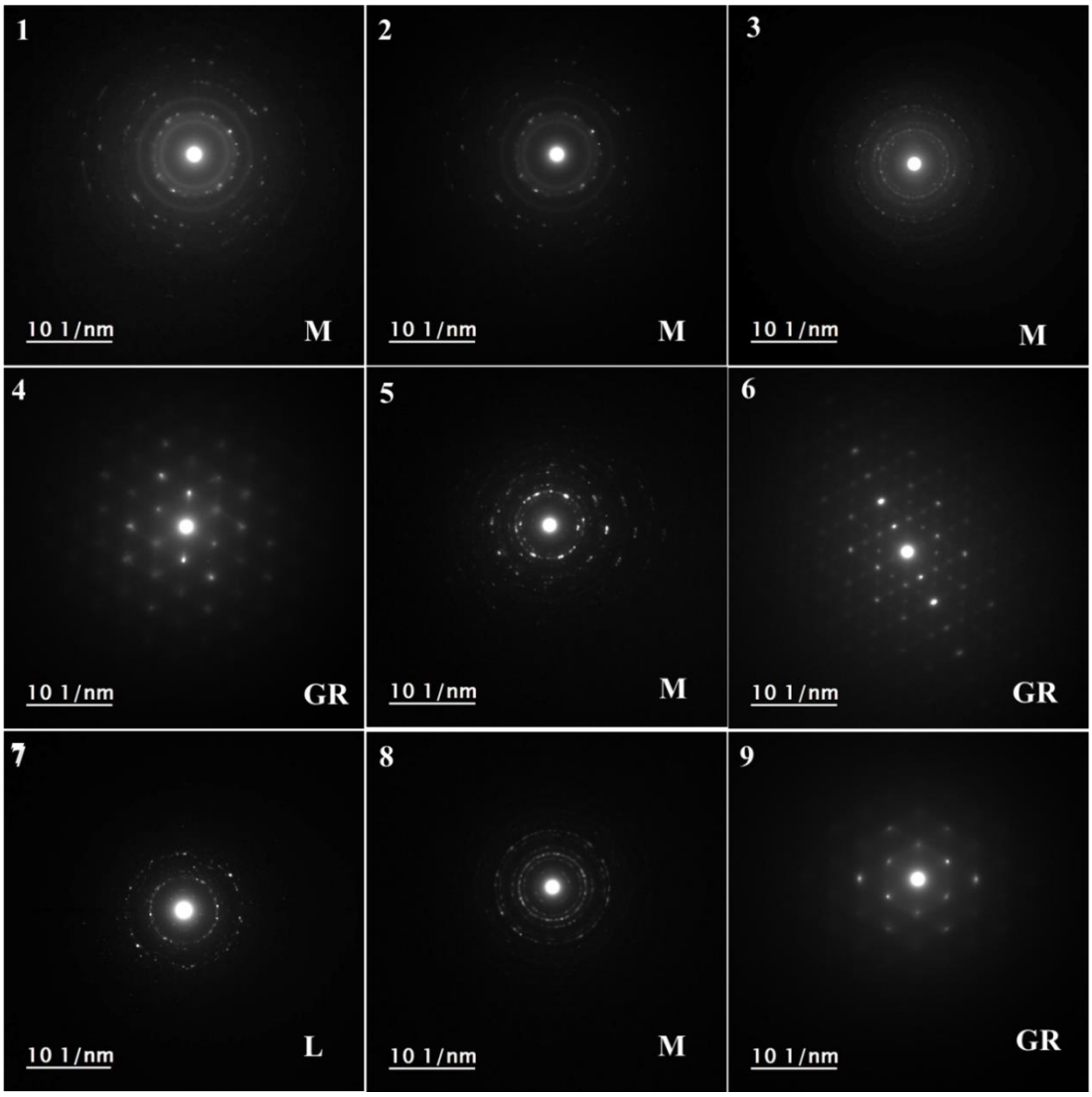

410 Figure 6. Electron diffraction patterns of selected areas from Fig. 5. Note: M,
411 magnetite/maghemite; GR, green rust; L, lepidocrocite.

412

413 To describe the mechanism underlying NA adsorption onto the 60 d-aged sample,
414 we applied a surface complexation model. We assumed that NA binds to two surface
415 hydroxy groups by involving its carboxylate and its keto-group as follows :(Cheng et
416 al. 2018)

$$2 \equiv FeOH + 2\ H^{+} + NA^{-} \rightleftharpoons (\equiv Fe)_2NA^{+} + 2\ H_2O \qquad \log {}^{NA}K \qquad (3)$$

Only the predominant phases were taken into consideration, and the mixed valent iron minerals (*i.e.*, magnetite and green rust) were supposed to exhibit similar behavior with respect to NA adsorption. Consequently, the magnetite parameters were used in the adsorption model in PW-anoxic-aged NZVI, GW1-anoxic-aged NZVI, and PW-oxic-aged NZVI samples. In the case of GW1-oxic-aged NZVI, the dominant phases were maghemite and lepidocrocite. NA adsorption to maghemite or lepidocrocite was first calculated, and all modeling parameters are shown in Table S2. The complexation of NA-Fe(II) was accounted for by using dissolved Fe(II) concentration as input parameters in this model.

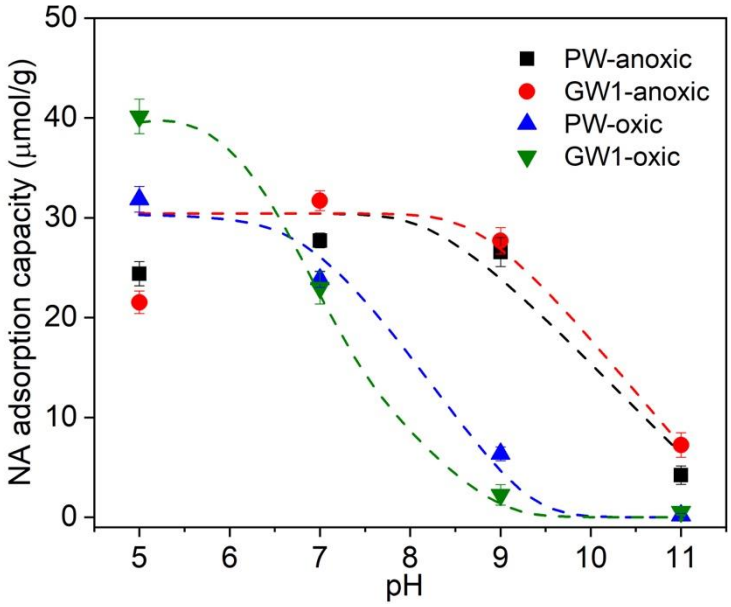

Figure 7. Experimental (symbols) and modelled (dashed lines) variation of nalidixic acid adsorption capacity of 60 d-aged NZVI sample with pH.

The model satisfactorily predicted the pH dependence of NA adsorption to aged NZVI but overestimated the NA adsorption at pH 5 in the anoxic-aged NZVI system (Fig. 7). This may be ascribed to the higher amount of dissolved Fe(II) under acidic conditions (see Fig. S8), which can affect NA-Fe (II) complexation in solution and thus ternary surface complexation (*i.e.*, surface−metal−ligand complex) (Cheng et al. 2018). We also simplified the model by considering only the predominant phase of mixed-valence oxides (magnetite) in anoxic-aged NZVI samples despite the co-existence of green rust. Nevertheless, the good accuracy of the experimental and modeling data at neutral and alkaline pH confirms the key role of surface-bound Fe(II) in the adsorption of NA.

In summary, aged NZVI samples showed a good capacity for NA adsorption, which increased with aging time. The high NA adsorption onto NZVI products at neutral to alkaline pH can be ascribed to the surface-bound Fe(II) in the secondary phases.

4. Conclusions

We investigated the aging and reactivity of NZVI in various groundwater systems. First, the nature of secondary iron phases resulting from NZVI aging in groundwater is strongly dependent on the groundwater composition. The final products of NZVI after reaction were mainly magnetite in pure water system, while green rust was predominant

in groundwater systems. With the aging process (up to 60 d), NZVI continuously lost its reductive activity in the PW system. However, in the groundwater this reductive ability was first enhanced in the short-term (1-5 d) and then declined at longer aging times. Adsorption tests revealed higher NA binding to NZVI aging products (~ 30 μmol/g at pH 7), while NA uptake by fresh NZVI was negligible. Notably, the adsorption capacity of NA generally increased with aging time, with unexpected greater adsorption at neutral to alkaline pH values. Additional experiments and surface complexation modeling suggested that this strong adsorption at alkaline conditions can be attributed to the surface-bound Fe(II). These results shed light on an overlooked aspect of interactions of environmental compounds with the secondary Fe minerals resulting from NZVI corrosion in groundwater. Our findings will also help to predict the fate of NZVI in groundwater, and the impact of the secondary Fe minerals on the mobility and transformation of contaminants in soil and groundwater.

Acknowledgments

This work was supported by the Institut Universitaire de France (IUF) and the National Research Foundation of Korea (NRF) grant funded by the Korean government (MSIT) (No. 2022R1A2C2005791). We gratefully acknowledge Isabelle Soutrel (LC/UV) and Vincent Dorcet (THEMIS platform, ScanMAT, UAR 2025 University of Rennes 1-CNRS; CPER-FEDER 2007–2014) for their assistance.

References

Adeleye, A, Keller, A.A., Miller, R., Lenihan, H. 2013. Persistence of commercial nanoscaled zero-valent iron (nZVI) and by-products. J. Nanopart. Res. 15, 1418-1422.

Alowitz, M.J. and Scherer, M.M., 2002. Kinetics of nitrate, nitrite, and Cr(VI) reduction by iron metal. Environ. Sci. Technol. 36(3), 299-306.

Araújo-Neto, R.P., Silva-Freitas, E.L., Carvalho, J.F., Pontes, T.R.F., Silva, K.L., Damasceno, I.H.M., Egito, E.S.T., Dantas, A.L., Morales, M.A. and Carriço, A.S., 2014. Monodisperse sodium oleate coated magnetite high susceptibility nanoparticles for hyperthermia applications. J. Magn. Magn. Mater. 364, 72-79.

Bae, S., Collins, R.N., Waite, T.D. and Hanna, K., 2018. Advances in surface passivation of nanoscale zerovalent iron (NZVI): A critical review. Environ. Sci. Technol. 52(21), 12010-12025.

Bae, S., Gim, S., Kim, H. and Hanna, K., 2016. Effect of $NaBH_4$ on properties of nanoscale zero-valent iron and its catalytic activity for reduction of *p*-nitrophenol. Appl. Catal., B 182, 541-549.

Bae, S. and Lee, W., 2014. Influence of riboflavin on nanoscale zero-valent iron reactivity during the degradation of carbon tetrachloride. Environ. Sci. Technol. 48(4), 2368-2376.

Chen, S., Belver, C., Li, H., Ren, L.Y., Liu, Y.D., Bedia, J., Gao, G.L. and Guan, J., 2018. Effects of pH value and calcium hardness on the removal of 1,1,1-trichloroethane by immobilized nanoscale zero-valent iron on silica based supports. Chemosphere 211, 102-111.

Cheng, W., Marsac, R. and Hanna, K., 2018. Influence of magnetite stoichiometry on the binding of emerging organic contaminants. Environ. Sci. Technol. 52(2), 467-473.

D. L. Parkhurst and C. A. J. Appelo., 1999. User's guide to PHREEQC (Version 2): A computer program for speciation, batch-reaction, one-dimensional transport, and inverse geochemical calculations.

Deng, J., Bae, S., Yoon, S., Pasturel, M., Marsac, R. and Hanna, K., 2020. Adsorption capacity of the corrosion products of nanoscale zerovalent iron for emerging contaminants. Environ. Sci. Nano. 7(12), 3773-3782.

Digiacomo, F., Tobler, D.J., Held, T. and Neumann, T., 2020. Immobilization of Cr(VI) by sulphate green rust and sulphidized nanoscale zerovalent iron in sand media: batch and column studies. Geochem. Trans. 21(1), 8.

Dong, H., Guan, X. and Lo, I.M.C., 2012. Fate of As(V)-treated nano zero-valent iron: Determination of arsenic desorption potential under varying environmental conditions by phosphate extraction. Water Res. 46(13), 4071-4080.

Dong, H., Jiang, Z., Deng, J., Zhang, C., Cheng, Y., Hou, K., Zhang, L., Tang, L. and

Zeng, G., 2018. Physicochemical transformation of Fe/Ni bimetallic nanoparticles during aging in simulated groundwater and the consequent effect on contaminant removal. Water Res. 129, 51-57.

Dong, Y., Sanford, R.A., Boyanov, M.I., Flynn, T.M., O'Loughlin, E.J., Kemner, K.M., George, S., Fouke, K.E., Li, S., Huang, D., Li, S. and Fouke, B.W., 2020. Controls on iron reduction and biomineralization over broad environmental conditions as suggested by the firmicutes orenia metallireducens strain Z6. Environ. Sci. Technol. 54(16), 10128-10140.

Eaton, A.D., Clesceri, L.S., Greenberg, A.E. and Franson, M.A.H., 1966. Standard methods for the examination of water and wastewater. Am J Public Health Nations Health. 56(3), 387-388.

Fadrus, H. and Malý, J., 1975. Suppression of iron(III) interference in the determination of iron(II) in water by the 1,10-phenanthroline method. The Analyst. 100, 549-554.

Génin, J.-M.R., Aïssa, R., Géhin, A., Abdelmoula, M., Benali, O., Ernstsen, V., Ona-Nguema, G., Upadhyay, C. and Ruby, C., 2005. Fougerite and FeII–III hydroxycarbonate green rust; ordering, deprotonation and/or cation substitution; structure of hydrotalcite-like compounds and mythic ferrosic hydroxide Fe(OH)(2+x). Solid State Sci. 7(5), 545-572.

Giasuddin, A., Kanel, S.R. and Choi, H., 2007. Adsorption of humic acid onto nanoscale zerovalent iron and its effect on arsenic removal. Environ. Sci. Technol. 41(6), 2022-2027.

Grasshoff, K., Kremling, K. and Ehrhardt, M., 2009. Methods of seawater analysis, John Wiley & Sons.

Hanna, K., 2007. Sorption of two aromatic acids onto iron oxides: Experimental study and modeling. J. Colloid Interface Sci. 309(2), 419-428.

Hwang, Y.H., Kim, D.G. and Shin, H.S., 2011. Mechanism study of nitrate reduction by nano zero valent iron. J. Hazard. Mater. 185(2-3), 1513-1521.

Joo, S.H., Feitz, A.J. and Waite, T.D., 2004. Oxidative degradation of the carbothioate herbicide, molinate, using nanoscale zero-valent iron. Environ. Sci. Technol. 38(7), 2242-2247.

Kanematsu, M., Waychunas, G.A. and Boily, J.-F.o. 2018. Silicate binding and precipitation on iron oxyhydroxides. Environ. Sci. Technol. 52(4), 1827-1833.

Kontoyannis, C.G. and Vagenas, N.V., 2000. Calcium carbonate phase analysis using XRD and FT-Raman spectroscopy. Analyst. 125(2), 251-255.

Krystofiak, E.S., Mattson, E.C., Voyles, P.M., Hirschmugl, C.J., Albrecht, R.M., Gajdardziska-Josifovska, M. and Oliver, J.A., 2013. Multiple morphologies of gold–magnetite heterostructure nanoparticles are effectively functionalized with protein for cell targeting. Microsc. Microanal. 19(4), 821-834.

548 Legrand, L., Mazerolles, L. and Chaussé, A., 2004. The oxidation of carbonate green
549 rust into ferric phases:solid-state reaction or transformation via solution. Geochim.
550 Cosmochim. Acta 68(17), 3497-3507.

551 Li, S., Wang, W., Liang, F. and Zhang, W.-x., 2017. Heavy metal removal using
552 nanoscale zero-valent iron (NZVI): Theory and application. J. Hazard. Mater. 322, 163-
553 171.

554 Liao, S., Wang, X., Yin, H., Post, J.E., Yan, Y., Tan, W., Huang, Q., Liu, F. and Feng,
555 X., 2020. Effects of Al substitution on local structure and morphology of lepidocrocite
556 and its phosphate adsorption kinetics. Geochim. Cosmochim. Acta 276, 109-121.

557 Libralato, G., Devoti, A.C., Ghirardini, A.V. and Vignati, D., 2017. Environmental
558 effects of NZVI for land and groundwater remediation. Springer International
559 Publishing.

560 Liu, T., Li, X. and Waite, T.D., 2014. Depassivation of aged Fe0 by divalent cations:
561 correlation between contaminant degradation and surface complexation constants.
562 Environ. Sci. Technol. 48(24), 14564-14571.

563 Meng, X., Korfiatis, G.P., Bang, S. and Bang, K.W., 2002. Combined effects of anions
564 on arsenic removal by iron hydroxides. Toxicol. Lett. 133(1), 103-111.

565 Mueller, N.C., Braun, J., Bruns, J., Černík, M., Rissing, P., Rickerby, D. and Nowack,
566 B., 2012. Application of nanoscale zero valent iron (NZVI) for groundwater
567 remediation in Europe. Environ. Sci. Pollut. R. 19(2), p.550-558.

568 Paterson, E., 2000. Iron oxides in the laboratory: Preparation and characterization. Clay
569 Miner. 27(3), 393-393.

570 Patnaik, P., 2017. Handbook of environmental analysis: Chemical pollutants in air,
571 water, soil, and solid wastes, Crc Press.

572 Phenrat, T., Thongboot, T. and Lowry, G.V., 2016. Electromagnetic induction of
573 zerovalent iron (ZVI) powder and nanoscale zero valent iron (NZVI) particles enhances
574 dechlorination of trichloroethylene in contaminated groundwater and soil: Proof of
575 concept. Environ. Sci. Technol. 50(2), 872-880.

576 Reinsch, B.C., Forsberg, B., Penn, R.L., Kim, C.S. and Lowry, G.V., 2010. Chemical
577 transformations during aging of zerovalent iron nanoparticles in the presence of
578 common groundwater dissolved constituents. Environ. Sci. Technol. 44(9), 3455.

579 Robberson, K.A., Waghe, A.B., Sabatini, D.A. and Butler, E.C., 2006. Adsorption of
580 the quinolone antibiotic nalidixic acid onto anion-exchange and neutral polymers.
581 Chemosphere. 63(6), 934-941.

582 Ryu, A., Jeong, S.-W., Jang, A. and Choi, H., 2011. Reduction of highly concentrated
583 nitrate using nanoscale zero-valent iron: Effects of aggregation and catalyst on
584 reactivity. Appl. Catal., B 105(1-2), 128-135.

585 Schöftner, P., Waldner, G., Lottermoser, W., Stöger-Pollach, M., Freitag, P. and
586 Reichenauer, T.G., 2015. Electron efficiency of NZVI does not change with variation
587 of environmental parameters. Sci. Total Environ. 535, 69-78.

588 Schwertmann, U. and Fechter, H., 1994. The formation of green rust and its
589 transformation to lepidocrocite. Clay Miner. 29(1), 87-92.

590 Standard, D. and ISO, B., 2004. Water quality: Determination of phosphorus—
591 ammonium molybdate spectrometric method. DS/EN ISO 6878, 2004.

592 Su, C. and Puls, R.W., 2001. Arsenate and arsenite removal by zerovalent iron: Effects
593 of phosphate, silicate, carbonate, borate, sulfate, chromate, molybdate, and nitrate,
594 relative to chloride. Environ. Sci. Technol. 35(22), 4562-4568.

595 Su, Y., Adeleye, A.S., Huang, Y., Sun, X., Dai, C., Zhou, X., Zhang, Y. and Keller, A.A.
596 2014. Simultaneous removal of cadmium and nitrate in aqueous media by nanoscale
597 zerovalent iron (nZVI) and Au doped nZVI particles. Water Res. 63, 102-111.

598 Su, Y.-f., Hsu, C.-Y. and Shih, Y.-h., 2012. Effects of various ions on the dechlorination
599 kinetics of hexachlorobenzene by nanoscale zero-valent iron. Chemosphere. 88(11),
600 1346-1352.

601 Tsarev, S., Collins, R.N., Ilton, E.S., Fahy, A. and Waite, T.D., 2017. The short-term
602 reduction of uranium by nanoscale zero-valent iron (NZVI): Role of oxide shell,
603 reduction mechanism and the formation of U(v)-carbonate phases. Environ. Sci. Nano.
604 4(6), 1304-1313.

605 Usman, M., Byrne, J.M., Chaudhary, A., Orsetti, S., Hanna, K., Ruby, C., Kappler, A.
606 and Haderlein, S.B., 2018. Magnetite and green rust: Synthesis, properties, and
607 environmental applications of mixed-valent iron minerals. Chem. Rev. 118(7), 3251-
608 3304.

609 Vincent, W.R., Schulman, S.G., Midgley, J.M., van Oort, W.J. and Sorel, R.H.A., 1981.
610 Prototropic and metal complexation equilibria of nalidixic acid in the physiological pH
611 region. Int. J. Pharmaceut. 9(3), 191-198.

612 Wei, Y.-T., Wu, S.-C., Chou, C.-M., Che, C.-H., Tsai, S.-M. and Lien, H.-L., 2010.
613 Influence of nanoscale zero-valent iron on geochemical properties of groundwater and
614 vinyl chloride degradation: A field case study. Water Res. 44(1), 131-140.

615 Westerhoff, P. and James, J., 2003. Nitrate removal in zero-valent iron packed columns.
616 Water Res. 37(8), 1818-1830.

617 Williams, A.G.B. and Scherer, M.M., 2001. Kinetics of Cr(VI) reduction by carbonate
618 green rust. Environ. Sci. Technol. 35(17), 3488-3494.

619 Xia, X., Ling, L. and Zhang, W.-x., 2017. Genesis of pure Se(0) nano- and micro-
620 structures in wastewater with nanoscale zero-valent iron (NZVI). Environ. Sci. Nano.
621 4(1), 52-59.

Xiao, S., Jin, Z., Dong, H., Xiao, J., Li, Y., Li, L., Li, R., Chen, J., Tian, R. and Xie, Q. 2022. A comparative study on the physicochemical properties, reactivity and long-term performance of sulfidized nanoscale zerovalent iron synthesized with different kinds of sulfur precursors and procedures in simulated groundwater. Water Res. 212, 118097.

Xie, Y. and Cwiertny, D.M., 2012. Influence of anionic cosolutes and pH on nanoscale zerovalent iron longevity: Time scales and mechanisms of reactivity loss toward 1,1,1,2-tetrachloroethane and Cr(VI). Environ. Sci. Technol. 46(15), 8365.

Xu, J., Marsac, R., Costa, D., Cheng, W., Wu, F., Boily, J.-F. and Hanna, K., 2017a. Co-binding of pharmaceutical compounds at mineral surfaces: Molecular investigations of dimer formation at goethite/water interfaces. Environ. Sci. Technol. 51(15), 8343-8349.

Xu, J., Marsac, R., Wei, C., Wu, F., Boily, J.F. and Hanna, K., 2017b. Cobinding of pharmaceutical compounds at mineral surfaces: Mechanistic modeling of binding and cobinding of nalidixic acid and niflumic acid at goethite surfaces. Environ. Sci. Technol. 51(20), 11617-11624.

Xu, J., Marsac, R., Wei, C., Wu, F., Boily, J.F. and Hanna, K., 2017c. Cobinding of pharmaceutical compounds at mineral surfaces: Mechanistic modeling of binding and cobinding of nalidixic acid and niflumic acid at goethite surfaces. Environ. Sci. Technol. 51(20), 11617-11624.

Zhou, L., Li, Z., Yi, Y., Tsang, E.P. and Fang, Z. 2022. Increasing the electron selectivity of nanoscale zero-valent iron in environmental remediation: A review. J. Hazard. Mater. 421, 126709.